Star-Shaped ESIPT-Active Mechanoresponsive Luminescent AIEgen and Its On−Off−On Emissive Response to Cu^{2+}/S$^{2−}$

Balamurugan Tharmalingam,[†] Moorthy Mathivanan,[†] Ganesh Dhamodiran,[†] Kailasam Saravana Mani,[†] Manikandan Paranjothy,[‡] and Balasubramanian Murugesapandian*,[†]

[†]Department of Chemistry, Bharathiar University, Coimbatore 641 046, Tamil Nadu, India
[‡]Department of Chemistry, Indian Institute of Technology Jodhpur, Jodhpur 342 037, Rajasthan, India

Ⓢ Supporting Information

ABSTRACT: Design and development of multifunctional materials have drawn incredible attraction in recent years. Herein, we report the design and construction of versatile star-shaped intramolecular charge transfer (ICT)-coupled excited-state intramolecular proton transfer (ESIPT)-active mechanoresponsive and aggregation-induced emissive (AIE) luminogen triaminoguanidine-diethylaminophenol (LH$_3$) conjugate from simple precursors triaminoguanidine hydrochloride and 4-(N,N-diethylamino)salicylaldehyde. Solvent-dependent dual emission in nonpolar to polar protic solvents implies the presence of ICT-coupled ESIPT features in the excited state. Aggregation-enhanced emissive feature of LH$_3$ was established in the CH$_3$CN/ water mixture. Furthermore, this compound exhibits mechanochromic fluorescence behavior upon external grinding. Fluorescence microscopy images of pristine, crystal, and crushed crystals confirm the naked-eye mechanoresponsive characteristics of LH$_3$. In addition, LH$_3$ selectively sensed a Cu^{2+} ion through a colorimetric and fluorescence "turn-off" route, and subsequently, the LH$_3$-Cu^{2+} ensemble could act as a selective and sensitive sensor for S$^{2−}$ in a "turn-on" fluorescence manner via a metal displacement approach. Reversible "turn-off−turn-on" features of LH$_3$ with Cu^{2+}/S$^{2−}$ ions were efficiently demonstrated to construct the IMPLICATION logic gate function. The Cu^{2+}/S$^{2−}$-responsive sensing behavior of LH$_3$ was established in the paper strip experiment also, which can easily be characterized by the naked eye under daylight as well as a UV lamp (λ = 365 nm).
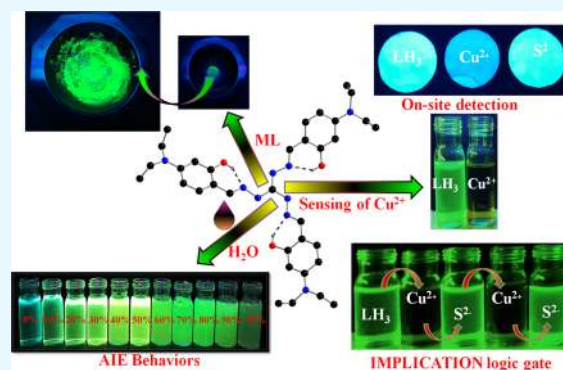
INTRODUCTION

Construction of multifunctional luminescent organic materials has attracted enormous amount of awareness over the past two decades for their extensive applications in diverse fields such as light-emitting devices, sensing, and biomedical applications.[1−8] Most of the conventional fluorescent materials exhibit weak or nonemissive features in the solid state (aggregation-caused quenching (ACQ)) and inhibit their real-time applications.[9,10] For the day-to-day application of these materials, reconstruction on functionality of these materials was needed to acquire the excellent solid-state emission. Recently, enormous effort has been devoted to develop the molecule that shows a weak emission in the solution state and enhanced emissive features in the aggregated state or solid state, and this behavior is known as aggregation-induced emission (AIE).[9,10] Various strategies have been utilized to enhance the luminescent behavior in the aggregated state or solid state, which included incorporation of an intramolecular charge transfer unit (ICT), twisted intramolecular charge transfer units (TICT),[11] and an excited-state intramolecular proton transfer (ESIPT) unit in the molecular architecture[12,13] and also restriction of intramolecular motions by aggregation or by putting it in a solid matrix. Among these, ESIPT-active fluorescent molecules have

attracted a lot due to multidisciplinary applications.[12−17] ESIPT is a four-step photochemical process; these molecules possess intramolecular hydrogen bonding between a proton donor such as hydroxyl or an amino group and proton acceptor such as imine nitrogen or carbonyl oxygen in the ground state. The proton transfer/relocation occurs between the proton donor and the proton acceptor unit in the excited state; that is, phototautomerization (enol form is converted into keto form) occurs in an ultrafast timescale under photoexcitation condition. These molecules normally characterized by intrinsic large Stokes shift, dual emission, and environment-dependent optical properties due to the influence of significant structural alteration occur in the excited state. An ESIPT-active molecule finds various applications in different fields such as electroluminescent materials, optical sensor, and laser applications.[12−17] Stimuli-responsive materials are organic or organometallic molecules that exhibit reversible optical properties with concomitant morphological changes upon undergoing external forces such as grinding, acid, thermal force, etc.[18−23]

In general, external stimuli altered the intra- and intermolecular interactions present in the systems, which ultimately influence the luminescence characteristics of the molecule. Hence, luminescent properties are directly related to the weaker interaction present in the molecular assemblies.[18a] Exclusively, construction of mechanoresponsive luminescent (MRL) materials is of great interest since grinding is used as external stimuli, which is facile and easy to handle also. It is well known that the diethylamino group could act as a strong electron-donating group, salicylaldimine moiety could act as an electron acceptor unit,[14c] and incorporation of these two units in a molecule induces strong donor−acceptor-based intramolecular charge transfer (ICT) features in the molecular systems. Diethylaminophenol-appended fluorescent molecules have attracted huge interest and find multiple applications in various fields.[24] Further, salicylaldehyde azine is one of the well-known classical ESIPT molecules due to the presence of strong intramolecular hydrogen bond between −OH (proton donor) and −N=CH (proton acceptor).[14,15] Design and development of the versatile molecules possessing ESIPT and ICT cores are very scarce.[15,25−31] In this vein, herein, we report the design and construction of versatile star-shaped luminescent organic molecule triaminoguanidine-diethylaminophenol conjugate (**LH₃**). The triaminoguanidine unit was used to construct the star-shaped architecture as well as to improve the proton-accepting capacity; diethylamino and salicylaldimine groups were employed to enrich a strong donor−acceptor feature in this system. The triaminoguanidine-diethylaminophenol conjugate **LH₃** comprises three imine and diethylaminophenol moieties, which are integrated through simple and facile hydrazone linkage by the Schiff base condensation reaction from carefully chosen building units. Further, we demonstrated the mechanoresponsive luminescence (MRL) behavior, aggregation-induced emissive features in the CH₃CN/water mixture, and reversible sensing characteristics of **LH₃** toward Cu^{2+}/S^{2-} ions. Reversible turn-off−turn-on features of **LH₃** with Cu^{2+}/S^{2-} ions were efficiently demonstrated to construct the IMPLICATION logic gate function. In addition, this reversible characteristic was established to develop a paper strip-based device for on-site applications.

RESULTS AND DISCUSSION

Design and construction of star-shaped organic molecules have received tremendous interest, owing to their interdisciplinary applications in multiple fields. Triaminoguanidine is a well-known building block for the construction of a star-shaped C₃-symmetric ligand or probe.[32,33] The triaminoguanidine scaffold has been utilized as a structural building unit for the construction of diethylaminophenol-functionalized, star-shaped organic molecules. Further, the star-shaped molecule was designed such that the periphery of the molecule comprises a strong electron-donating diethylamino group and the inner core is built up with ESIPT-active acceptor units (OH···N=CH). As a result, the expected molecule holds three donor−acceptor units integrated with the ESIPT-active core. The molecule was synthesized by the simple condensation reaction between triaminoguanidine hydrochloride with 4-diethylamino salicylaldehyde in moderate yield (**LH₃**) (Scheme 1). The formation of the compound was confirmed by spectral studies and single-crystal XRD analysis. The newly designed molecule has carbon-centered donor−acceptor conjugates, where it holds three strong electron-donating

Scheme 1. Synthesis of LH₃
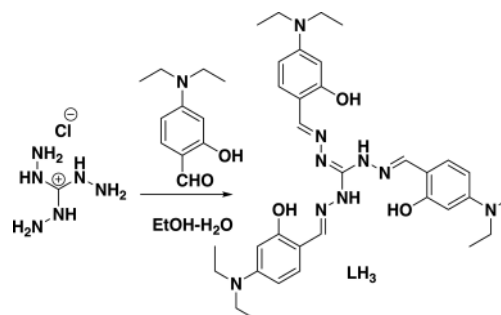
diethylamino groups in the circumference of the system, which are linked to the center carbon via facile hydrazone linkages.

Photophysical Properties. Incorporation of the strong donor−acceptor unit besides proton transfer moieties in the molecules will deliver the photophysical properties more dominated by a combination of ICT and ESIPT phenomena.[12−17] To authenticate the projected photophysical properties of compound **LH₃**, absorption and emission studies have been carried out using various solvents with different polarities. The compound divulged a broad absorption band at 430 nm, which is characteristic of a charge transfer band (Figure 1A). Upon excitation at 430 nm, the molecule exhibited dual emission in various nonpolar and polar aprotic solvents with a strong band around 470−480 nm and shoulder around 530 nm (Figure 1B and Figure S4). The existence of dual emission in different solvents is a characteristic of ESIPT behavior present in the current systems. However, in polar protic solvents (methanol or ethanol), the compound exhibited a strong emission at a longer-wavelength (520 nm) region along with a weaker emission at a shorter-wavelength (470 nm) region (Figure 1B). It is well known that the polar protic solvent (methanol) inhibits the ESIPT process by intermolecular hydrogen bonding with the molecule.[15,34] But the appearance of an intense ESIPT peak at a longer-wavelength region in methanol/ethanol might be attributed by the formation of eight-membered rings between the intermolecular hydrogen-bonded alcohol and molecule.[32a,35] Further, owing to the presence of proton transfer (ESIPT) and charge transfer groups (ICT) in molecules, the ICT process was expected to occur between the diethylamino group and imino acceptor unit, which could further increase the proton-accepting ability of imine nitrogen from the intramolecularly hydrogen-bonded phenolic OH group (ESIPT) and lead to the ICT-coupled ESIPT process in the excited state.[15] Hence, large Stoke-shifted ∼100 nm lower energy band at a higher wavelength was assigned to the charge-coupled proton-transferred keto form (K*), and the less Stoke-shifted ∼40−50 nm higher energy band was assigned to the enol form (E*) in the excited species.[15] The fluorescence quantum yield (Φ) for **LH₃** was measured in different solvents with varying polarities, and results are given in Table S1. Due to the presence of a strong electron-donating group in the periphery of the system, it facilitates the electron transfer from the diethylamino group to hydrogen-bonded imine nitrogen and led to the ICT-coupled ESIPT in the excited state.[14,15,25,26]

In addition, to elucidate ESIPT behavior, the density functional theory calculations were carried out to estimate the energy gap of the highest occupied molecular orbital (HOMO) and lowest unoccupied molecular orbital (LUMO)
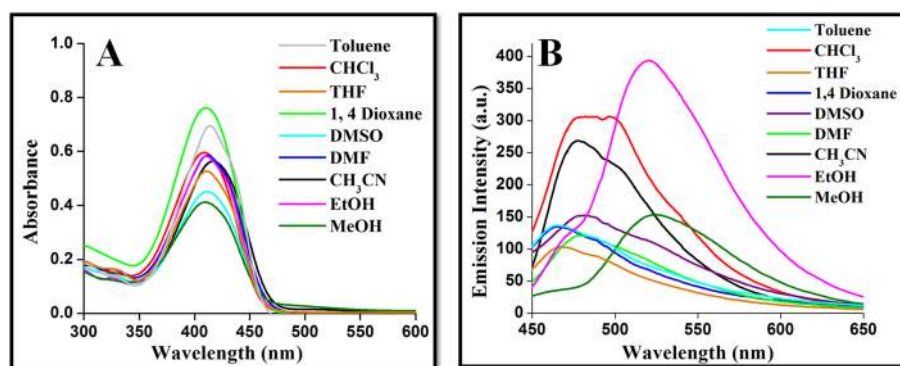
Figure 1. (A) Absorption spectra of **LH$_3$** (5 μM) in different organic solvents. (B) Emission spectra of **LH$_3$** (5 μM) in different organic solvents (λ_{ex} = 430 nm).
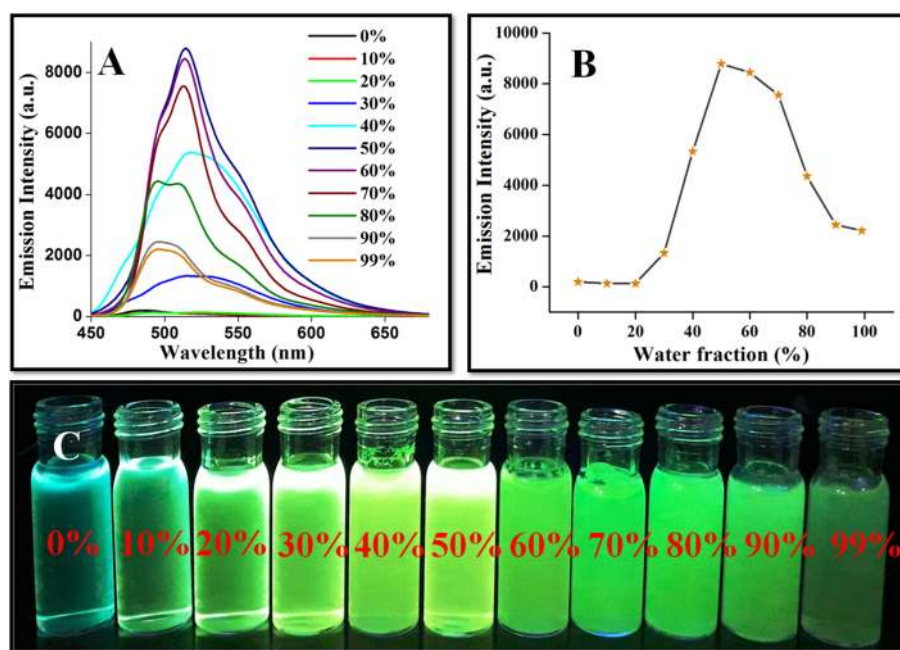
Figure 2. (A) Emission spectra of **LH$_3$** in CH$_3$CN/water mixtures with increasing water fractions (λ_{ex} = 430 nm). (B) Emission intensity of **LH$_3$** in different CH$_3$CN/water fraction. (C) Fluorescence photo of **LH$_3$** with increasing water fractions (0−99%) under a UV lamp (365 nm).

for the keto and enol forms of **LH$_3$**. Using the B3LYP/6-31G* level of electronic structure theory, the geometries of the two molecules were energy-minimized. Normal mode frequency calculations were performed to make sure that the stationary point computed is a minimum and not a saddle point. Calculations were performed using the electronic structure theory program NWChem,[36] and the computed energy-minimized geometries of the two molecules are shown in Figure S5. Electronic structure calculations (including zero-point energy corrections) show that the enol form is more stable by 24.902 kcal/mol with respect to the keto form. The computed HOMO−LUMO energy gap of keto and enol forms are 2.57 and 2.76 eV, respectively.

AIE Characteristics of LH$_3$. In general, molecules containing freely rotatable and quickly isomerizable units undergo nonradiative deactivation of excited states easily.[9−13] Hence, restriction or prohibition of nonradiative relaxation through inhibition of molecular motions such as rotation or isomerization via molecular aggregation leads to enhanced emission behavior.[9−13] Due to the presence of donor−acceptor conjugates with free rotatable N−N bond and an easily isomerizable CH═N group in molecule **LH$_3$**, the effect of molecular aggregation on photophysical properties was investigated.[14] The influence of aggregation on optical properties of compound **LH$_3$** was studied by UV−vis and emission measurements in a CH$_3$CN/water solvent mixture with varying water content (0 to 99%), and the observations are shown in Figure 2. Upon excitation at 430 nm, **LH$_3$** exhibits weak emission as a broad peak around 485 nm with shoulder at 535 nm in pure CH$_3$CN. When the amount of water content was 40%, the dual peak was merged as a broad band, and at 50%, it started to appear as a strong major peak at 513 nm with two shoulders at 494 and 553 nm. The ∼46-fold enhancement in emission intensity clearly indicates the formation of aggregates. After 50% water content, the emission intensity was slowly decreased with increase in water content. This observed behavior clearly indicates the formation of an organic nanoaggregate at 50% water content.[5a,13c,26] Formation of the nanoaggregate was further ascertained by dynamic light scattering (DLS), field emission scanning electron microscopy (FE-SEM) measurements, and quantum yield calculations (Table S2). Compound **LH$_3$** shows a level-off tail in UV−vis

absorption measurements (Figure S6) when water content was above 50% in the CH$_3$CN/water mixture, further attesting the characteristic features of the aggregate formation.[13c,26] AIE characteristics of **LH$_3$** in the CH$_3$CN/water mixture can be easily visualized through the naked eye under a UV lamp as well as in daylight (Figure S7), which indicates the aggregate formation behavior of **LH$_3$** in the CH$_3$CN/water mixture (Figure 2C).

In dilute CH$_3$CN, **LH$_3$** displays weak emission due to the presence of a free rotatable N—N single bond and an easily isomerizable CH=N moiety in **LH$_3$**, which destroys the excited state through nonradiative decay and produces a weak or nonemissive behavior. Upon increasing the water fraction, **LH$_3$** starts to precipitate as aggregates due to the low solubility, which hinder the various types of intramolecular motions and display an enhanced emission at 50% water content.[9−13] Further, comparative results from emission measurements in highly viscous glycerol/CH$_3$CN and nonviscous water/CH$_3$CN mixtures (Figure S8) inferred that the restriction of intramolecular rotation (RIR) mechanism also operated in addition to ICT-coupled ESIPT phenomenon for enhanced emission in this compound.[9−13] In addition, increment in emission intensity was observed in an ice-cold solution of CH$_3$CN, DMSO, and toluene compared to emission measurements at room temperature, which clearly indicates the presence of RIR mechanism (Figure S9). FE-SEM and DLS measurements were also used to validate the formation of aggregates. The DLS result divulges that the particle size of an aggregate at 50% is larger than that of an aggregate at 99% of water content in the CH$_3$CN/water mixture (Figure S10). Morphological changes were also observed for **LH$_3$** in pure CH$_3$CN and aggregates at 50% of water content in the CH$_3$CN/water mixture, which are confirmed by FE-SEM images (Figure S11).

Mechanoresponsive Luminescent Behavior of LH$_3$. In general, AIE- and ESIPT-active donor−acceptor molecules have a stimuli-responsive behavior.[18−24] Hence, the mechanoresponsive emissive behavior of **LH$_3$** was investigated by solid-state emission measurements. The pristine sample exhibits a broad weak emissive band at 497 nm, whereas after external grinding, the ground sample shows enhanced emission intensity with a red shift in peak position at 513 nm (Figure S12). The bathochromic shift of ∼16 nm from the pristine state to the ground state was evidenced by luminescent color change from yellow to greenish yellow under a UV lamp (λ = 365 nm) (Figure 3 and Video S1). Upon grinding, the

Figure 3. Photographic images of pristine and ground samples under a UV lamp.

emission intensity was increased, and it remained the same as long as there is no disruption on it, while even scraping the ground sample by a spatula caused a decrease in the emission intensity (Video S2). Further recrystallization of the ground sample produces the original state of the molecule. Congruently, quantum yield increases from 0.92 to 13.54% upon grinding. Powder X-ray diffraction (PXRD) studies of pristine- and ground-state samples support the existence of

morphology changes from the crystalline nature of the pristine state to the amorphous nature of the ground state. The pristine sample produces the strong and well-resolved intense line (crystalline state) in PXRD, while the ground sample exhibits (amorphous) broad peaks (Figure S13). Further, SEM analysis was carried out to validate the morphological changes that occur from the pristine state to the ground state upon grinding (Figure S14). These observations visibly indicates that the facile simple mechanical force produces the morphological changes as well as destroys the weak intermolecular interaction and transforms the twisted propeller structure into a somewhat planar structure with a change in color as well as emission intensity.[14c] The physical state-dependent luminescent behaviors of crystals, pristine, and crushed crystals were studied under a fluorescence microscope as well as in daylights (Figure S15), and results indicate that fluorescent behavior was enhanced in crushed crystals compared to crystal, and the as-synthesized sample and its corresponding fluorescence microscopy images are represented in Figure 4.

Solid-State Structure of LH$_3$. To correlate the ESIPT and AIE behavior of the compound **LH$_3$** with molecular arrangements, single-crystal analysis was carried out. The fluorescent crystal was obtained from slow diffusion of *n*-hexane into a compound in chloroform. Figure 5A shows the molecular structure of the compound. The molecule is crystallized as a neutral molecule. It consists of three wings of 4-(Et$_2$N)-C$_6$H$_3$—2-OH—CH=N—NH connected to the central carbon atom through the N—C bond that led to the star-shaped propeller molecular structure. In each wing, the strong intramolecular hydrogen bonding was observed between the —OH group from diethylaminophenolic moieties and imine nitrogen of triaminoguanidine moiety —C(NHN=C)$_3$— (1.901, 1.925, and 1.92 Å) and led to a six-membered ring (Figure 5A). Further, this intramolecular hydrogen bonding assists the ESIPT process in the excited state. Normally, triaminoguanidinium-based Tris Schiff base compounds formed as guanidinium salts,[32,33] but this molecule was formed/crystalized as a neutral molecule, which may be due to the strong electron-donating nature of the diethylamino group present in the periphery of the system. All the three wings are not present in the same plane and are twisted to each other by 37.055° (planes 1 and 2), 35.420° (planes 1 and 3), and 38.762° (planes 2 and 3) (Figure S16). Subsequently, the whole molecule adopts the propeller-shaped conformation in the solid state (Figure 5B and Figure S16A). Further, this molecule forms a dimer by strong C···C interaction (3.154 Å, Figure 5B) between the center carbon atoms of two neighboring molecules, and through C−H···π interaction, it adopts a one-dimensional polymeric chain (Figure 5c and Figure S16B). The presence of propeller-shaped conformation in **LH$_3$** inhibits the aggregation-caused quenching by destroying the strong π−π stacking interaction between diethylamino phenol rings.[22−24] Here, the propeller-shaped conformation of **LH$_3$**, intramolecular hydrogen bonding between OH···N and intermolecular CH···O, and CH···π interaction plays a predominant role in AIE and mechanochromic luminescent behaviors.

Analytical Studies of LH$_3$. Recently, considerable interest in the development of an ESIPT-based turn-on or turn-off sensor for selective detection of metal ions is based on inhibition of the ESIPT process through the coordination of metal ions.[37,38] Herein, **LH$_3$** has three binding sites, each binding site consisting of a phenolic hydroxyl group and imine

Figure 4. Fluorescence microscopy images of (A) crystals, (B) pristine, (C) crushed crystals of **LH₃**.
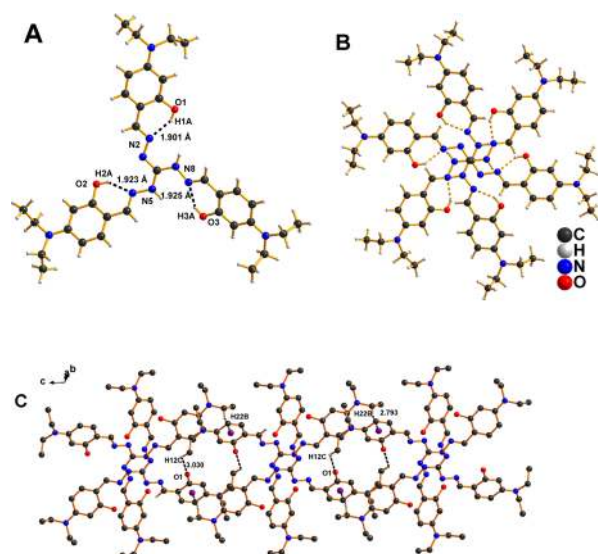
Figure 5. (A) Molecular structure, (B) dimeric structure, and (C) one-dimensional polymeric chain structure of **LH₃**.

nitrogen and NH from a triaminoguanidine unit. Hence, the metal-sensing performance of **LH₃** has been investigated by UV−vis absorption and emission measurements toward various metal ions such as Ag(I), Al(III), Ca(II), Cd(II),

Co(II), Cu(II), Cr(III), Fe(III), Mn(II), Mg(II), Na(I), Ni(II), Pb(II), Hg(II), and Zn(II) in CH_3CN/H_2O (10 mM Tris−HCl; pH = 7.2; 9:1, v/v) mixture. The corresponding metal ions were used as their perchlorate or nitrate salts. The absorption spectral result of the probe **LH₃** with and without metal ions indicates that only Cu^{2+} induces changes in the absorption band, whereas no changes were observed with the rest of the metal ions (Figure S17A). Absorption titration experiments were carried out between the probe and Cu^{2+}. The incremental addition of Cu^{2+} to the probe produces the red shift in position of the absorption band from 420 to 460 nm with a clear isosbestic point at 440 nm (Figure S17B). This result confirms the formation of new species. Further, upon excitation at 430 nm, **LH₃** (20 μM) exhibits a sharp peak around 470 nm in CH_3CN/H_2O (10 mM Tris−HCl; pH = 7.2; 9:1, v/v) mixture. The outcome from the emission measurement of **LH₃** with and without metal ions confirms that the probe shows selective sensitivity toward Cu^{2+} over the other metal ions via a fluorescence turn-off mode (Figure 6A). Interestingly, during the gradual addition of Cu^{2+} to the probe, emission intensity was completely quenched after the addition of 3 equiv of Cu^{2+} ions (Figure 6B). This titration result indicates the formation of 1:3 complexes between the probe and Cu^{2+} ion. Further, results from a Job plot[39] (Figure S19) and Benesi−Hildebrand analysis[40] also confirm that the 1:3 complex formation occurs between **LH₃** and Cu^{2+}. In addition, mass spectral analysis of in situ-prepared **LH₃**-Cu^{2+} also
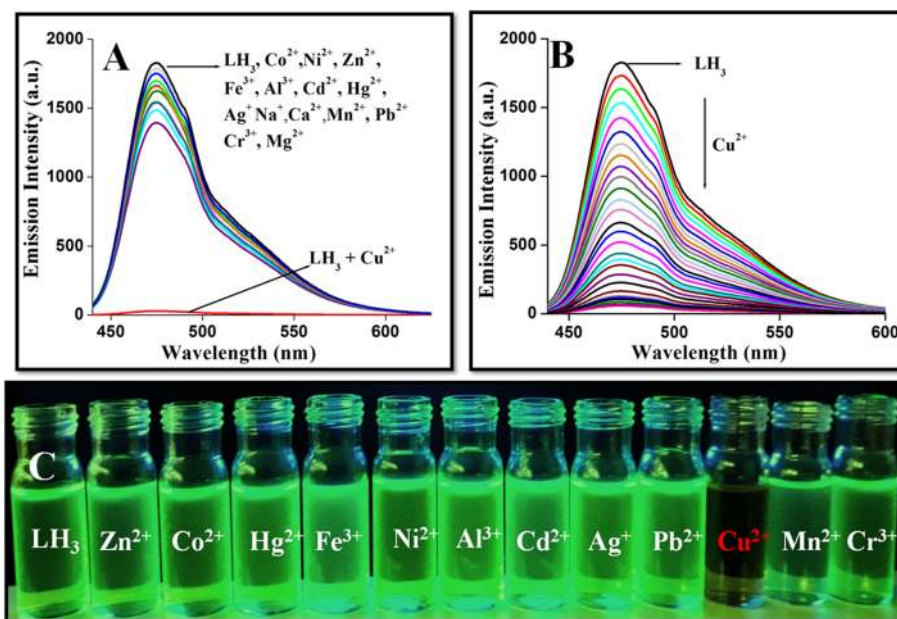
Figure 6. (A) Fluorescence spectra of **LH₃** (CH_3CN/H_2O; 9:1, v/v; Tris−HCl, pH = 7.2) with various metal ions (5 equiv) (λ_{ex} = 430 nm). (B) Fluorescence spectra of **LH₃** (CH_3CN/H_2O; 9:1, v/v; 10 mM Tris−HCl, pH = 7.2) with increasing concentration of Cu^{2+} ion (λ_{ex} = 430 nm). (C) Photograph of **LH₃** with various metal ions under UV light at 365 nm.
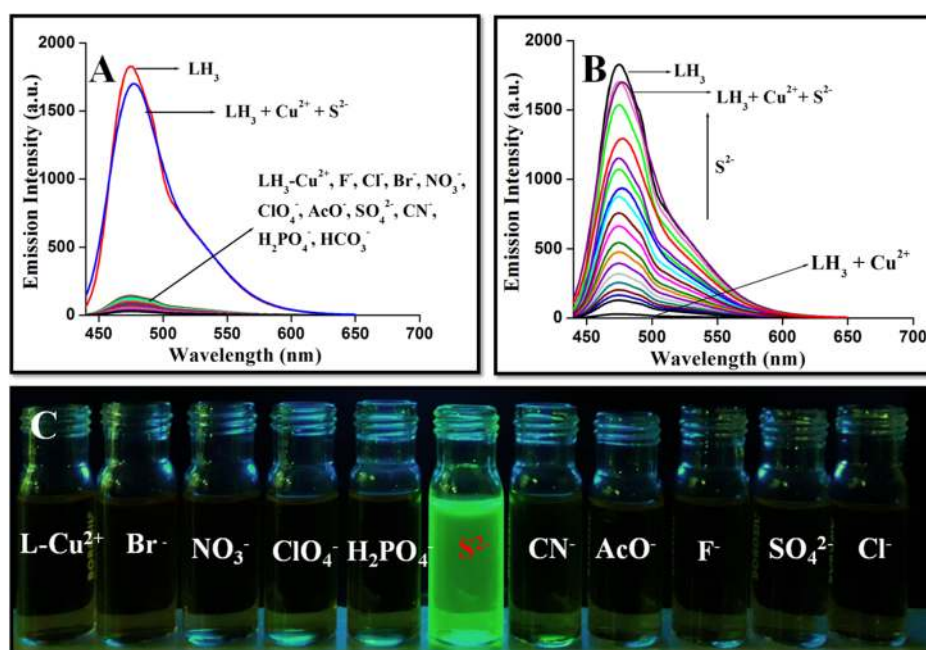
Figure 7. (A) Emission changes of **LH₃** with different anions (5 equiv) in the presence of Cu²⁺. (B) Emission titration of **LH₃**-Cu²⁺ with S²⁻ anion. (C) Colorimetric detection of S²⁻ by **LH₃**-Cu²⁺.

confirms the 1:3 stoichiometric ratio, and it shows m/z values for $[LCu_3Cl_3(DMSO) + 2H^+]^{2+}$ at 502.56 (Figure S20). The IR spectral changes of the probe with and without Cu²⁺ ions clearly demonstrate the coordination of imine nitrogen to the metal ion (Figure S21). The deprotonation of −OH groups occurs during the formation of **LH₃**-Cu²⁺ ensembles, which inhibit the ESIPT process and resulted in the gradual decrease in the emission intensity.[41] Further drastic decrease in the quantum yield was observed from 0.25 to 0.08% upon addition of Cu²⁺ to the probe with a naked eye-detectable color change from fluorescent green to nonemissive under UV light (365 nm). It is interesting to note that the limit of detection value of **LH₃** for Cu²⁺ was calculated as 2.33×10^{-7} M (23.3 ppm) (Figure S22), which is below the permissible value of Cu²⁺ in drinking water according to WHO.[42] Further, the association constant was found to be 4.78×10^6 M⁻¹, and it implies that the probe has strong binding affinity to the Cu²⁺ ion. Further, to access the selectivity of **LH₃** toward the Cu²⁺ ion, competitive photophysical measurements were carried out for **LH₃** with other metal ions in the presence of Cu²⁺, and the results are represented in Figure S23. The result clearly implies that the probe has strong selectivity toward Cu²⁺ over the other metal ions and it could act as a fluorescent turn-off sensor for the Cu²⁺ ion. The quenching behavior of Cu²⁺ might be due to the paramagnetic nature of Cu²⁺, inhibition of ESIPT, and chelation-enhanced quenching.[41,43]

It is well known that Cu²⁺ ions have strong affinity toward the S²⁻ anion,[44,45,49−51] and this validates the selective sensing behavior of **LH₃**-Cu²⁺ assembly toward S²⁻ through displacement approach. The anion-sensing characteristic of in situ-prepared **LH₃**-Cu²⁺ ensemble was evaluated by absorption and fluorescence experiments in the presence of various anions. The response of absorption and emission titration measurements indicates that gradual addition of S²⁻ to **LH₃**-Cu²⁺ induces the regaining of photophysical characteristics of the ligand via displacement of Cu²⁺ from **LH₃**-Cu²⁺ by formation of the Cu−S complex with bare probe-resulted turn-on

emission as well as colorimetric changes (Scheme S1, Figure 7, and Figure S25). The S²⁻ response by the composite probe **LH₃**-Cu²⁺ is visible via color changes from colorless to bluish green under a UV lamp (Figure 7C). Further, competitive experiments confirm the selective sensing of S²⁻ by the **LH₃**-Cu²⁺ ensemble. Hence, **LH₃**-Cu²⁺ could act as a colorimetric as well as fluorescent turn-on sensor exclusively for S²⁻ (Figure 7 and Figure S25). The limit-of-detection value and association constant of **LH₃**-Cu²⁺ ensembles toward S²⁻ were found to be 2.05×10^{-7} M and 4.43×10^6 M⁻¹, respectively. The above results authenticate that the probe **LH₃** could be used as a reversible and reusable sensor for Cu²⁺ and S²⁻ ions (Figure 8 and Figure S26). Further, the recycle ability of **LH₃** was checked by consecutive addition of Cu²⁺ and S²⁻ ions to **LH₃**, and their associated colorimetric responses under a UV lamp clearly indicate the recycle characteristic and stability of **LH₃** for more than five cycles and future utilization for sensing applications (Figure S26). The practical application of the
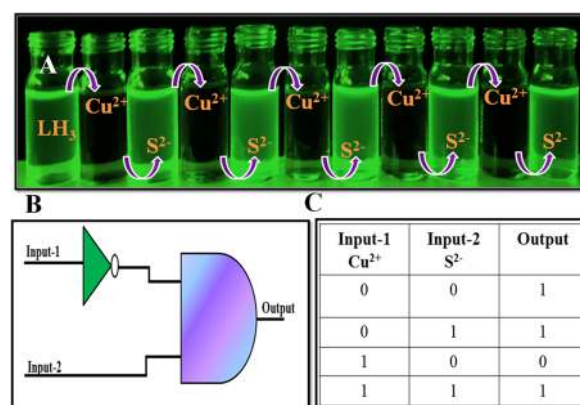
Figure 8. (A) Reversible sensing nature of **LH₃** toward Cu²⁺ and S²⁻ under a UV lamp. (B, C) Construction of truth table of IMPLICATION logic circuit.

probe **LH₃** for the detection of Cu^{2+} and S^{2-} ions was carried out in real water samples such as drinking water and tap water, and the results are presented in Tables S3 and S4.

Construction of IMPLICATION Logic Gate. The reversible and selective on−off−on sensing characteristics of **LH₃** toward Cu^{2+} and S^{2-} induced us to explore the construction of molecular switches by our systems.[45a,46−49] Herein, the introduction of Cu^{2+} and S^{2-} ions to the probe **LH₃** is abbreviated as inputs 1 and 2, and resultant emission intensity is denoted as an output. The decrement of emission intensity is denoted as output "0", and regaining of emission intensity is denoted as output "1". The emissive nature of the probe makes output as "1" even in the absence of both inputs. Addition of Cu^{2+} quenches the emissive nature of the probe; hence, the output is 0. Introduction of S^{2-} to the above solution (**LH₃**-Cu^{2+}) regains the emission, and the resultant output is 1, whereas addition of S^{2-} to the bare probe causes no change in emission, leading to output "1". The reversible sensing characteristics of **LH₃** toward Cu^{2+} and S^{2-} satisfied the requirements of IMPILICATION logic gate, and the corresponding truth table is given in (Figure 8).[45a,49]

On-Site Detection of Cu^{2+} and S^{2-}. Exclusive colorimetric and selective turn-off sensing behavior of **LH₃** toward Cu^{2+} was established by paper strip experiments.[52] Under a UV lamp, the bluish green color was changed to blue color in the presence of a Cu^{2+} ion, whereas the other metal ion did not produce any changes in the **LH₃**-coated filter paper (Figure 9A). Further, a **LH₃**-Cu^{2+}-coated paper was utilized to
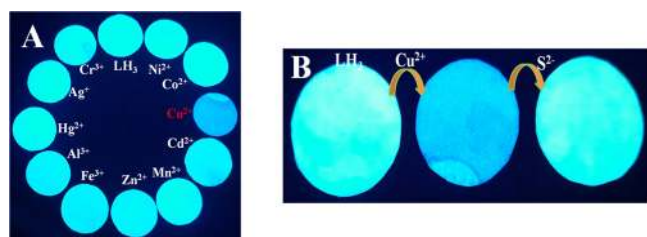
Figure 9. (A) Photographic images of paper strip-based selective naked-eye detection of Cu^{2+} by an **LH₃**-coated filter paper under a UV lamp. (B) On−off−on sensing nature of **LH₃**-coated filter paper for detection of Cu^{2+} and S^{2-}.

selectively discriminate S^{2-} ions over the other anions by converting to the original color of an **LH₃**-coated paper, which is easily visible to the naked eye under a UV lamp (Figure 9B). These results clearly indicate that the **LH₃**-coated paper can act as a sensing device for the on-site detection of Cu^{2+} and S^{2-} ions.

CONCLUSIONS

In summary, a star-shaped propeller-like diethylaminophenoltriaminoguanidine conjugate was synthesized from readily accessible building blocks. The molecules exhibit polarity-dependent dual emissions in various solvents. In polar protic solvents, **LH₃** exhibits dominant ICT-coupled ESIPT emission. The aggregation-enhanced emission features of **LH₃** were demonstrated in the CH_3CN/water mixture. The mechanochromic luminescence characteristic of **LH₃** was established by grinding and confirmed by PXRD experiments of ground and unground samples. In addition, **LH₃** selectively detects the Cu^{2+} ion in a colorimetric and fluorescent turn-off manner. In situ-prepared **LH₃**-Cu^{2+} ensembles selectively detect S^{2-} ions

over the various anions through the colorimetric and fluorescent turn-on pathway. Reversibility of **LH₃** toward Cu^{2+} and S^{2-} is stable over more than five cycles. Further, the sensing feature of **LH₃** was utilized to develop the IMPILICATION logic gate function and on-site analysis of Cu^{2+} and S^{2-} ions by a paper strip-based device.

GENERAL METHODS

4-Diethylaminosalicylaldehyde and guanidine hydrochloride were procured from Sigma Aldrich. Analytical grade solvents and reagents were purified by standard methods and used for the synthesis. FT-IR spectra for **LH₃** and **LH₃**-Cu^{2+} were measured by using a JASCO FTIR 4100 instrument with a frequency range of 4000 to 400 cm^{-1}. $CDCl_3$ was used as a solvent to measure the ^1H and ^{13}C NMR spectra of **LH₃** on a Bruker Avance (400 MHz for ^1H and 100 MHz for ^{13}C) instrument. Tetramethylsilane was used as a standard for the presentation of chemical shifts (δ values, ppm), and coupling constants are reported in hertz (Hz). The following abbreviations are used: singlet (s), doublet (d), triplet (t), and quartet (q). The melting point of the sample was determined on a Guna melting point apparatus and was uncorrected. They are expressed in °C. A JASCO V-630 UV− Visible spectrophotometer was used to measure the absorption spectral measurements by using 1.0 cm path length Quartz cuvettes. For all the absorption measurements, 1×10^{-3} M stock solution was prepared, and during the experiments, 5 μL was taken in a cuvette and diluted to 2.5 mL by suitable solvents.

A JASCO FP-8300 spectrofluorometer equipped with a 1.0 cm path length quartz cuvette was used for the emission spectral experiments and excited at 430 nm. The emission spectra were monitored in the wavelength range of 450−800 nm. All the measurements were carried out at ambient temperature (25 °C). For solvent-dependent emission measurements, 1×10^{-3} M stock solution was prepared in the respective solvent, and 125 μL was taken in a cuvette and diluted to 2.5 mL by appropriate solvents. For sensing measurements, 1×10^{-3} M stock solution was prepared in CH_3CN, and 20 μL was diluted to 2.5 mL by using CH_3CN/ H_2O (9:1, v/v) (10 mM Tris−HCl-buffered solution, pH 7.2). Stock solutions for metal salts were prepared in distilled water with a concentration of 1×10^{-3} M. A HORIBA FluoroMax was used for solid-state fluorescence measurements.

Dynamic light scattering (DLS) experiments are recorded by the Malvern Zetasizer Nano ZS instrument equipped with a 4.0 mW He−Ne laser operating at a wavelength of 633 nm at room temperature. Field emission scanning electron microscopy images were taken from FEI Quanta 250. High-resolution mass spectra were recorded on an Exactive Plus EMR Orbitrap mass spectrometer using the electron spray ionization (ESI) technique. A CKX 41 (Olympus) fluorescence microscope was used to capture the fluorescent images of crystal, pristine, and crushed crystals.

A Bruker D8 QUEST diffractometer was used to measure the single-crystal X-ray diffraction data of **LH₃**. Measurement was carried out at 296(2) K using a graphite-monochromatic Mo Kα radiation (λ = 0.71073 Å). The Bruker SAINT Software package[53] using a narrow-frame algorithm was used to integrate the data. Absorption correction was performed using SADABS.[54] Structure was solved with multiscan method using SHELXT. The structure was refined by full-matrix least squares on F2 using the SHELXL-2014/7 program.[55] Non-

hydrogen atoms were refined freely with anisotropic displacement parameters. The hydrogen atoms were placed in calculated positions and refined with a riding model.

Formula: $C_{34}H_{47}N_9O_3$; $F_w = 629.81$; crystal system: triclinic; space group: P-1; $a = 10.8574(7)$ Å, $b = 13.1942(9)$ Å, $c = 13.9240(9)$ Å; $\alpha = 104.519(2)°$, $\beta = 99.677(2)°$, $\gamma = 109.459(2)°$; $V = 1750.1(2)$ Å^3; $Z = 2$; $D_c = 1.197$ g/cm^3; absorption coefficient: 0.079 mm^{-1}; $F(000) = 678$; $T = 296(2)$ K; $\theta_{max} = 27.18°$; reflections collected: 45,243; independent reflections: 7718; R1 = 0.0753; wR2 = 0.1620; R1 = 0.1861; wR2 = 0.1918; goodness-of-fit on F^2 = 1.243.

Synthesis of LH$_3$. Triaminoguanidinium chloride was prepared according to the following literature method.[32] Triaminoguanidinium chloride (0.230 g, 1.64 mmol) was dissolved in a mixture of ethanol (5 mL) and water (2.5 mL) at 80 °C, and it was stirred for 10 min. To the above solution, 4-diethylaminosalicylaldehyde (0.983 g, 5.10 mmol) in ethanol was added dropwise, and the mixture was allowed to reflux at 80 °C for 12 h. Then, the resulting yellow precipitate was filtered off, washed with cold ethanol, and dried. Yield: 0.450 g, 40%; mp 220−221 °C; IR(KBr) v(cm^{-1}): 3327(−OH), 2969 (−NH), 1618(−CH=N−); ^{1}H NMR (400 MHz, CDCl$_3$) (ppm): δ 11.83 (s, 3H), 8.48 (s, 3H), 7.12 (d, J = 12.0 Hz, 3H), 6.23 (s, 6H), 3.41 (q, 12H), 1.23 (t, 18H); ^{13}C NMR(100 MHz, CDCl$_3$) (ppm): δ 161.1, 160.9, 151.3, 133.3, 106.9, 103.6, 97.8, 44.5, 12.4; HR-MS (m/z): [$C_{34}H_{47}N_9O_3$] + H$^+$: calcd, 630.3875; found, 630.3881.

■ ASSOCIATED CONTENT

Ⓢ Supporting Information

The Supporting Information is available free of charge on the ACS Publications website at DOI: 10.1021/acsomega.9b00845.

> Characterization of the compound **LH$_3$** and various data of spectral experiments (PDF)
>
> Crystallographic file from the compound **LH$_3$** (CIF)
>
> Luminescent color change of the ground sample from yellow to greenish yellow under a UV lamp (MP4)
>
> Scraping of the ground sample using a spatula (MP4)

■ AUTHOR INFORMATION

Corresponding Author

*E-mail: mpandian@gmail.com. Fax: +91-422-2422387. Tel: +91-422-2428312.

ORCID Ⓞ

Kailasam Saravana Mani: 0000-0001-5795-3652
Manikandan Paranjothy: 0000-0002-4126-6206
Balasubramanian Murugesapandian: 0000-0002-7096-9816

Notes

The authors declare no competing financial interest.

■ ACKNOWLEDGMENTS

■ REFERENCES

(1) (a) Baldo, M. A.; O'Brien, D. F.; You, Y.; Shoustikov, A.; Sibley, S.; Thompson, M. E.; Forrest, S. R. Highly efficient phosphorescent emission from organic electroluminescent devices. *Nature* **1998**, *395*, 151−154. (b) Saragi, T. P. I.; Spehr, T.; Siebert, A.; Fuhrmann-Lieker, T.; Salbeck, J. Spiro Compounds for Organic Optoelectronics. *Chem. Rev.* **2007**, *107*, 1011−1065. (c) Wu, K.-C.; Ku, P.-J.; Lin, C.-S.; Shih, H.-T.; Wu, F.-I.; Huang, M.-J.; Lin, J.-J.; Chen, I.-C.; Cheng, C.-H. The Photophysical Properties of Dipyrenylbenzenes and Their Application as Exceedingly Efficient Blue Emitters for Electroluminescent Devices. *Adv. Funct. Mater.* **2008**, *18*, 67−75. (d) Lin, G.; Peng, H.; Chen, L.; Nie, H.; Luo, W.; Li, Y.; Chen, S.; Hu, R.; Qin, A.; Zhao, Z.; Tang, B. Z. Improving Electron Mobility of Tetraphenylethene-Based AIEgens to Fabricate Nondoped Organic Light-Emitting Diodes with Remarkably High Luminance and Efficiency. *ACS Appl. Mater. Interfaces* **2016**, *8*, 16799−16808.

(2) (a) Ashton, T. D.; Jolliffe, K. A.; Pfeffer, F. M. Luminescent probes for the bioimaging of small anionic species *in vitro* and *in vivo*. *Chem. Soc. Rev.* **2015**, *44*, 4547−4595. (b) Sun, S.-K.; Wang, H.-F.; Yan, X.-P. Engineering Persistent Luminescence Nanoparticles for Biological Applications: From Biosensing/Bioimaging to Theranostics. *Acc. Chem. Res.* **2018**, *51*, 1131−1143.

(3) (a) Gunnlaugsson, T.; Glynn, M.; Tocci, G. M.; Kruger, P. E.; Pfeffer, F. M. Anion Recognition and Sensing in Organic and Aqueous Media Using Luminescent and Colorimetric Sensors. *Coord. Chem. Rev.* **2006**, *250*, 3094−3117. (b) De Silva, A. P.; Gunaratne, H. Q. N.; Gunnlaugsson, T.; Huxley, A. J. M.; McCoy, C. P.; Rademacher, J. T.; Rice, T. E. Signaling Recognition Events with Fluorescent Sensors and Switches. *Chem. Rev.* **1997**, *97*, 1515−1566.

(4) Lochenie, C.; Schötz, K.; Panzer, F.; Kurz, H.; Maier, B.; Puchtler, F.; Agarwal, S.; Köhler, A.; Weber, B. Spin-Crossover Iron(II) Coordination Polymer with Fluorescent Properties: Correlation between Emission Properties and Spin State. *J. Am. Chem. Soc.* **2018**, *140*, 700−709.

(5) (a) Wang, Z.; Gui, C.; Zhao, E.; Wang, J.; Li, X.; Qin, A.; Zhao, Z.; Yu, Z.; Tang, B. Z. Specific Fluorescence Probes for Lipid Droplets Based on Simple AIEgens. *ACS Appl. Mater. Interfaces* **2016**, *8*, 10193−10200. (b) Kwok, R. T. K.; Leung, C. W. T.; Lam, J. W. Y.; Tang, B. Z. Biosensing by luminogens with aggregation induced emission characteristics. *Chem. Soc. Rev.* **2015**, *44*, 4228−4238.

(6) Ni, J.-S.; Lee, M. M. S.; Zhang, P.; Gui, C.; Chen, Y.; Wang, D.; Yu, Z.-Q.; Kwok, R. T. K.; Lam, J. W. Y.; Tang, B. Z. SwissKnife-Inspired Multifunctional Fluorescence Probes for Cellular Organelle Targeting Based on Simple AIEgens. *Anal. Chem.* **2019**, *91*, 2169−2176.

(7) Zhu, C.; Kwok, R. T. K.; Lam, J. W. Y.; Tang, B. Z. Aggregation-Induced Emission; A Trailblazing Journey to the Field of Biomedicine. *ACS Appl. Bio Mater.* **2018**, *1*, 1768−1786.

(8) Dang, D.; Liu, H.; Wang, J.; Chen, M.; Liu, Y.; Sung, H. H.-Y.; Williams, I. D.; Kwok, R. T. K.; Lam, J. W. Y.; Tang, B. Z. Highly Emissive AIEgens with Multiple Functions: Facile Synthesis, Chromism, Specific Lipid Droplet Imaging, Apoptosis Monitoring, and In Vivo Imaging. *Chem. Mater.* **2018**, *30*, 7892−7901.

(9) (a) Hong, Y.; Lam, J. W. Y.; Tang, B. Z. Aggregation-induced emission. *Chem. Soc. Rev.* **2011**, *40*, 5361−5388. (b) Mei, J.; Leung, N. L. C.; Kwok, R. T. K.; Lam, J. W. Y.; Tang, B. Z. Aggregation-Induced Emission: Together We Shine, United We Soar! *Chem. Rev.* **2015**, *115*, 11718−11940.

(10) (a) Chen, G.; Li, W.; Zhou, T.; Peng, Q.; Zhai, D.; Li, H.; Yuan, W. Z.; Zhang, Y.; Tang, B. Z. Conjugation-Induced Rigidity in Twisting Molecules: Filling the Gap Between Aggregation-Caused Quenching and Aggregation-Induced Emission. *Adv. Mater.* **2015**, *27*, 4496−4501. (b) Hu, R.; Leung, N. L. C.; Tang, B. Z. AIE

Macromolecules: Syntheses, Structures and Functionalities. *Chem. Soc. Rev.* **2014**, *43*, 4494−4562.

(11) (a) Hu, R.; Lager, E.; Aguilar-Aguilar, A.; Liu, J.; Lam, J. W. Y.; Sung, H. H. Y.; Williams, I. D.; Zhong, Y.; Wong, K. S.; Peña-Cabrera, E.; Tang, B. Z. Twisted Intramolecular Charge Transfer and Aggregation-Induced Emission of BODIPY Derivatives. *J. Phys. Chem. C* **2009**, *113*, 15845−15853. (b) Ghosh, R.; Palit, D. K. Effect of Donor-Acceptor Coupling on TICT Dynamics in the Excited States of Two Dimethylamine Substituted Chalcones. *J. Phys. Chem. A.* **2015**, *119*, 11128−11137.

(12) Sedgwick, A. C.; Wu, L.; Han, H.-H.; Bull, S. D.; He, X.-P.; James, T. D.; Sessler, J. L.; Tang, B. Z.; Tian, H.; Yoon, J. Excited-state intramolecular proton-transfer (ESIPT) based fluorescence sensors and imaging agents. *Chem. Soc. Rev.* **2018**, *47*, 8842−8880.

(13) (a) Sturala, J.; Etherington, M. K.; Bismillah, A. N.; Higginbotham, H. F.; Trewby, W.; Aguilar, J. A.; Bromley, E. H. C.; Avestro, A.-J.; Monkman, A. P.; McGonigal, P. R. Excited-State Aromatic Interactions in the Aggregation-Induced Emission of Molecular Rotors. *J. Am. Chem. Soc.* **2017**, *139*, 17882−17889. (b) Leung, N. L. C.; Xie, N.; Yuan, W.; Liu, Y.; Wu, Q.; Peng, Q.; Miao, Q.; Lam, J. W. Y.; Tang, B. Z. Restriction of Intramolecular Motions: The General Mechanism behind Aggregation-Induced Emission. *Chem. − Eur. J.* **2014**, *20*, 15349−15353. (c) Li, K.; Feng, Q.; Niu, G.; Zhang, W.; Li, Y.; Kang, M.; Xu, K.; He, J.; Hou, H.; Tang, B. Z. Benzothiazole-Based AIEgen with Tunable Excited-State Intramolecular Proton Transfer and Restricted Intramolecular Rotation Processes for Highly Sensitive Physiological pH Sensing. *ACS Sens.* **2018**, *3*, 920−928.

(14) (a) Tang, W.; Xiang, Y.; Tong, A. Salicylaldehyde Azines as Fluorophores of Aggregation-Induced Emission Enhancement Characteristics. *J. Org. Chem.* **2009**, *74*, 2163−2166. (b) Peng, L.; Zheng, Y.; Wang, X.; Tong, A.; Xiang, Y. Photoactivatable Aggregation-Induced Emission Fluorophores with Multiple-Color Fluorescence and Wavelength-Selective Activation. *Chem. − Eur. J.* **2015**, *21*, 4326−4332. (c) Chen, X.; Wei, R.; Xiang, Y.; Zhou, Z.; Li, K.; Song, P.; Tong, A. Organic Crystalline Solids Response to Piezo/thermo Stimulus: Donor-Acceptor (D-A) Attached Salicylaldehyde Azine Derivatives. *J. Phys. Chem. C* **2011**, *115*, 14353−14359.

(15) Jana, S.; Dalapati, S.; Guchhait, N. Proton Transfer Assisted Charge Transfer Phenomena in Photochromic Schiff Bases and Effect of −NEt$_2$ Groups to the Anil Schiff Bases. *J. Phys. Chem. A.* **2012**, *116*, 10948−10958.

(16) (a) Murale, D. P.; Kim, H.; Choi, W. S.; Churchill, D. G. Highly Selective Excited State Intramolecular Proton Transfer (ESIPT)-Based Superoxide Probing. *Org. Lett.* **2013**, *15*, 3946−3949. (b) Zhao, J.; Ji, S.; Chen, Y.; Guo, H.; Yang, P. Excited State Intramolecular Proton Transfer (ESIPT): From Principal Photophysics to the Development of New Chromophores and Applications in Fluorescent Molecular Probes and Luminescent Materials. *Phys. Chem. Chem. Phys.* **2012**, *14*, 8803−8817. (c) Kwon, J. E.; Park, S. Y. Advanced Organic Optoelectronic Materials: Harnessing Excited-State Intramolecular Proton Transfer (ESIPT) Process. *Adv. Mater.* **2011**, *23*, 3615−3642.

(17) (a) Song, Z.; Kwok, R. T. K.; Zhao, E.; He, Z.; Hong, Y.; Lam, J. W. Y.; Liu, B.; Tang, B. Z. A Ratiometric Fluorescent Probe Based on ESIPT and AIE Processes for Alkaline Phosphatase Activity Assay and Visualization in Living Cells. *ACS Appl. Mater. Interfaces* **2014**, *6*, 17245−17254. (b) Barman, S.; Mukhopadhyay, S. K.; Gangopadhyay, M.; Biswas, S.; Dey, S.; Pradeep Singh, N. D. Coumarin−benzothiazole−chlorambucil (Cou-Benz-Cbl) Conjugate: an ESIPT Based pH Sensitive Photoresponsive Drug Delivery System. *J. Mater. Chem. B* **2015**, *3*, 3490−3497.

(18) (a) Wang, C.; Li, Z. Molecular conformation and packing: their critical roles in the emission performance of mechanochromic fluorescence materials. *Mater. Chem. Front.* **2017**, *1*, 2174−2194. (b) Yang, Z.; Chi, Z.; Mao, Z.; Zhang, Y.; Liu, S.; Zhao, J.; Aldred, M. P.; Chi, Z. Recent advances in mechano-responsive luminescence of tetraphenylethylene derivatives with aggregation-induced emission properties. *Mater. Chem. Front.* **2018**, *2*, 861−890.

(19) (a) Zhao, W.; He, Z.; Peng, Q.; Lam, J. W. Y.; Ma, H.; Qiu, Z.; Chen, Y.; Zhao, Z.; Shuai, Z.; Dong, Y.; Tang, B. Z. Highly sensitive switching of solid-state luminescence by controlling intersystem crossing. *Nat. Commun.* **2018**, *9*, 3044. (b) Li, Y.; Ma, Z.; Li, A.; Xu, W.; Wang, Y.; Jiang, H.; Wang, K.; Zhao, Y.; Jia, X. A Single Crystal with Multiple Functions of Optical Waveguide, Aggregation-Induced Emission, and Mechanochromism. *ACS Appl. Mater. Interfaces* **2017**, *9*, 8910−8918. (c) Wu, J.; Cheng, Y.; Lan, J.; Wu, D.; Qian, S.; Yan, L.; He, Z.; Li, X.; Wang, K.; Zou, B.; You, J. Molecular Engineering of Mechanochromic Materials by Programmed C-H Arylation: Making a Counterpoint in the Chromism Trend. *J. Am. Chem. Soc.* **2016**, *138*, 12803−12812.

(20) (a) Dong, Y. Q.; Lam, J. W. Y.; Tang, B. Z. Mechanochromic Luminescence of Aggregation-Induced Emission Luminogens. *J. Phys. Chem. Lett.* **2015**, *6*, 3429−3436. (b) Wang, A.; Fan, R.; Wang, P.; Fang, R.; Hao, S.; Zhou, X.; Zheng, X.; Yang, Y. Research on the Mechanism of Aggregation-Induced Emission through Supramolecular Metal−Organic Frameworks with Mechanoluminescent Properties and Application in Press-Jet Printing. *Inorg. Chem.* **2017**, *56*, 12881−12892.

(21) Butler, T.; Morris, W. A.; Samonina-Kosicka, J.; Fraser, C. L. Mechanochromic Luminescence and Aggregation Induced Emission of Dinaphthoylmethane β-Diketones and Their Boronated Counterparts. *ACS Appl. Mater. Interfaces* **2016**, *8*, 1242−1251.

(22) (a) Wang, Y.; Xu, D.; Gao, H.; Wang, Y.; Liu, X.; Han, A.; Zhang, C.; Zang, L. Twisted Donor−Acceptor Cruciform Luminophores Possessing Substituent-Dependent Properties of Aggregation-Induced Emission and Mechanofluorochromism. *J. Phys. Chem. C* **2018**, *122*, 2297−2306. (b) Zhao, J.; Chi, Z.; Zhang, Y.; Mao, Z.; Yang, Z.; Ubba, E.; Chi, Z. Recent progress in the mechanofluorochromism of cyanoethylene derivatives with aggregation-induced emission. *J. Mater. Chem. C* **2018**, *6*, 6327−6353. (c) Gao, H.; Xu, D.; Liu, X.; Han, A.; Zhou, L.; Zhang, C.; Yang, Y.; Li, W. Tetraphenylethene modified β-ketoiminate boron complexes bearing aggregation-induced emission and mechanofluorochromism. *RSC Adv.* **2017**, *7*, 1348−1356.

(23) (a) Gao, H.; Xu, D.; Wang, Y.; Wang, Y.; Liu, X.; Han, A.; Zhang, C. Effects of alkyl chain length on aggregation-induced emission, self-assembly and mechanofluorochromism of tetraphenylethene modified multifunctional β-diketonate boron complexes. *Dyes Pigm.* **2018**, *150*, 59−66. (b) Wang, Y.; Xu, D.; Gao, H.; Wang, Y.; Liu, X.; Han, A.; Zhang, C.; Zang, L. Mechanofluorochromic properties of aggregation-induced emission-active tetraphenylethene-containing cruciform luminophores. *Dyes Pigm.* **2018**, *156*, 291−298.

(24) (a) Chandrasekhar, V.; Azhakar, R.; Murugesapandian, B.; Senapati, T.; Bag, P.; Pandey, M. D.; Maurya, S. K.; Goswami, D. Synthesis, Structure, and Two-Photon Absorption Studies of a Phosphorus-Based Tris Hydrazone Ligand (S)P[N(Me)N═CH-C$_6$H$_3$-2-OH-4-N(CH$_2$CH$_3$)$_2$]$_3$ and Its Metal Complexes. *Inorg. Chem.* **2010**, *49*, 4008−4016. (b) Han, T.; Feng, X.; Chen, D.; Dong, Y. A diethylaminophenol functionalized Schiff base: Crystallization-induced emission-enhancement, switchable fluorescence and application for security printing and data storage. *J. Mater. Chem. C* **2015**, *3*, 7446−7454. (c) Yang, M.; Zhang, Y.; Zhu, W.; Wang, H.; Huang, J.; Cheng, L.; Zhou, H.; Wu, J.; Tian, Y. Difunctional chemosensor for Cu(II) and Zn(II) based on Schiff base modified anthryl derivative with aggregation-induced emission enhancement and piezochromic characteristics. *J. Mater. Chem. C* **2015**, *3*, 1994−2002. (d) Sun, J.; Han, J.; Liu, Y.; Duan, Y.; Han, T.; Yuan, J. Mechanochromic luminogen with aggregation-induced emission: implications for ink-free rewritable paper with high fatigue resistance and low toxicity. *J. Mater. Chem. C* **2016**, *4*, 8276−8283.

(25) Kothavale, S.; Sekar, N. A New Series of Highly Fluorescent Blue-Green Emitting, Imidazole-Based ICT-ESIPT Compounds: Detail Experimental and DFT Study of Structural and Donating Group Effects on Fluorescence Properties. *ChemistrySelect* **2017**, *2*, 7691−7700.

(26) Santhiya, K.; Sen, S. K.; Natarajan, R.; Shankar, R.; Murugesapandian, B. D-A-D Structured Bis-acylhydrazone Exhibiting

Aggregation Induced Emission, Mechanochromic Luminescence, and Al(III) Detection. *J. Org. Chem.* **2018**, *83*, 10770−10775.

(27) (a) Song, H.; Kuang, Z.; Wang, X.; Guo, Y.; Guo, Q.; Zhang, H.; Xia, A. Solvent Polarity Dependent Excited State Dynamics of 2′-Hydroxychalcone Derivatives. *J. Phys. Chem. C* **2018**, *122*, 15108−15117. (b) Seo, J.; Kim, S.; Park, S. Y. Strong Solvatochromic Fluorescence from the Intramolecular Charge-Transfer State Created by Excited-State Intramolecular Proton Transfer. *J. Am. Chem. Soc.* **2004**, *126*, 11154−11155.

(28) Lin, W.-C.; Fang, S.-K.; Hu, J.-W.; Tsai, H.-Y.; Chen, K.-Y. Ratiometric Fluorescent/Colorimetric Cyanide-Selective Sensor Based on Excited-State Intramolecular Charge Transfer-Excited-State Intramolecular Proton Transfer Switching. *Anal. Chem.* **2014**, *86*, 4648−4652.

(29) Zhou, P.; Han, K. Unraveling the Detailed Mechanism of Excited-state Proton Transfer. *Acc. Chem. Res.* **2018**, *51*, 1681−1690.

(30) Zhao, N.; Li, Y.; Jia, Y.; Li, P. Identifying the Role of Intramolecular Charge Transfer and Excited-State Proton Transfer in Fluorescence Mechanism for an Azido-Based Chemosensor. *J. Phys. Chem. C* **2018**, *122*, 26576−26583.

(31) Kothavale, S.; Erande, Y.; Sekar, N. Triphenylamine-Based Bis- and Tris-ESIPT Compounds and Their Boron Complexes: Synthesis, Photophysical Properties and DFT Study of ICT and ESIPT Emissions. *ChemistrySelect* **2017**, *2*, 5013−5024.

(32) (a) Pallavi, P.; Kumar, V.; Hussain, M. D.W.; Patra, A. Excited-State Intramolecular Proton Transfer-Based Multifunctional Solid-State Emitter: A Fluorescent Platform with "Write-Erase-Write" Function. *ACS Appl. Mater. Interfaces* **2018**, *10*, 44696−44705. (b) Kumar, V.; Sk, B.; Kundu, S.; Patra, A. Dynamic and static excimer: a versatile platform for single component white-light emission and chelation-enhanced fluorescence. *J. Mater. Chem. C* **2018**, *6*, 12086−12094. (c) Plaul, D.; Böhme, M.; Ostrovsky, S.; Tomokowicz, Z.; Görls, H.; Haase, W.; Plass, W. Modeling Spin Interactions in a Triangular Cobalt(II) Complex with Triaminoguanidine Ligand Framework: Synthesis, Structure, and Magnetic Properties. *Inorg. Chem.* **2018**, *57*, 106−119.

(33) (a) Mukherjee, S.; Desai, A. V.; Inamdar, A. I.; Manna, B.; Ghosh, S. K. Selective Detection of 2,4,6-Trinitrophenol (TNP) by a π-Stacked Organic Crystalline Solid in Water. *Cryst. Growth Des.* **2015**, *15*, 3493−3497. (b) Zhou, Y.; Li, Z.-X.; Zang, S.-Q.; Zhu, Y.-Y.; Zhang, H.-Y.; Hou, H.-W.; Mak, T. C. W. A Novel Sensitive Turn-on Fluorescent Zn²⁺ Chemosensor Based on an Easy To PrepareC₃-Symmetric Schiff-Base Derivative in 100% Aqueous Solution. *Org. Lett.* **2012**, *14*, 1214−1217. (c) Jiang, X.-J.; Li, M.; Lu, H.-L.; Xu, L.-H.; Xu, H.; Zang, S.-Q.; Tang, M.-S.; Hou, H.-W.; Mak, T. C. W. A Highly SensitiveC₃-Symmetric Schiff-Base Fluorescent Probe for Cd²⁺. *Inorg. Chem.* **2014**, *53*, 12665−12667. (d) Datta, B. K.; Kar, C.; Das, G. A novel C₃ᵥ- symmetric completely water soluble turn-on chemo sensor for Cd²⁺ and the resultant complex for iodide anion in aqueous medium. *Sens. Actuators, B* **2014**, *204*, 474−479.

(34) Khan, A. U.; Kasha, M. Mechanism of Four-Level Laser Action in Solution Excimer and Excited-State Proton-Transfer Cases. *Proc. Natl. Acad. Sci. U. S. A.* **1983**, *80*, 1767−1770.

(35) Ghiggino, K. P.; Scully, A. D.; Leaver, I. H. Effect of Solvent on Excited-State Intramolecular Proton Transfer in Benzotriazole Photostabilizers. *J. Phys. Chem. A* **1986**, *90*, 5089−5093.

(36) Valiev, M.; Bylaska, E. J.; Govind, N.; Kowalski, K.; Straatsma, T. P.; Van Dam, H. J. J.; Wang, D.; Nieplocha, J.; Apra, E.; Windus, T. L.; et al. NWChem: A Comprehensive and Scalable Open-source Solution for Large Scale Molecular Simulations. *Comput. Phys. Commun.* **2010**, *181*, 1477−−1489.

(37) Sinha, S.; Chowdhury, B.; Ghosh, P. A Highly Sensitive ESIPT-Based Ratiometric Fluorescence Sensor for Selective Detection of Al³⁺. *Inorg. Chem.* **2016**, *55*, 9212−9220.

(38) (a) Asthana, S. K.; Kumar, A.; Neeraj; Shweta; Hira, S. K.; Manna, P. P.; Upadhyay, K. K. Brightening Quinolineimines by Al³⁺ and Subsequent Quenching by PPi/PA in Aqueous Medium: Synthesis, Crystal Structures, Binding Behavior, Theoretical and cell Imaging Studies. *Inorg. Chem.* **2017**, *56*, 3315−3323. (b) Maity, D.;

Kumar, V.; Govindaraju, T. Reactive Probes for Ratiometric Detection of Co²⁺ and Cu⁺ Based on Excited-State Intramolecular Proton Transfer Mechanism. *Org. Lett.* **2012**, *14*, 6008−6011. (c) Xu, Y.; Pang, Y. Zinc binding-induced near-IR emission from excited-state intramolecular proton transfer of a bis(benzoxazole) derivative. *Chem. Commun.* **2010**, *46*, 4070−4072.

(39) Skoog, D. A.; West, D. M.; Holler, F. J. *Fundamentals of Analytical Chemistry*; 5th edition, WB Saunders Co, Holt, Rinehart and Winston: United States, 1988.

(40) Benesi, H. A.; Hildebrand, J. H. A spectrophotometric investigation of the interaction of iodine with aromatic hydrocarbons. *J. Am. Chem. Soc.* **1949**, *71*, 2703−2707.

(41) (a) Wang, H.; Shi, D.-L.; Li, J.; Tang, H.-Y.; Li, J.; Guo, Y. A facile fluorescent probe with a large Stokes shift for sequentially detecting copper and sulfide in 100% aqueous solution and imaging them in living cells. *Sens. Actuators, B* **2018**, *256*, 600−608. (b) Mani, K. S.; Rajamanikandan, R.; Murugesapandian, B.; Shankar, R.; Sivaraman, G.; Ilanchelian, M.; Rajendran, S. P. Coumarin based hydrazone as an ICT-based fluorescence chemosensor for the detection of Cu²⁺ ions and the application in HeLa cells. *Spectrochim. Acta, Part A* **2019**, *214*, 170−176.

(42) World Health Organization *Guidelines for Drinking-Water Quality*; WHO Press: Geneva, Switzerland, 2008, p. 188

(43) Jung, H. S.; Kwon, P. S.; Lee, J. W.; Kim, J. I.; Hong, C. S.; Kim, J. W.; Yan, S.; Lee, J. Y.; Lee, J. H.; Joo, T.; Kim, J. S. Coumarin-Derived Cu²⁺-Selective Fluorescence Sensor: Synthesis, Mechanisms, and Applications in Living Cells. *J. Am. Chem. Soc.* **2009**, *131*, 2008−2012.

(44) (a) Sasakura, K.; Hanaoka, K.; Shibuya, N.; Mikami, Y.; Kimura, Y.; Komatsu, T.; Ueno, T.; Terai, T.; Kimura, H.; Nagano, T. Development of a Highly Selective Fluorescence Probe for Hydrogen Sulfide. *J. Am. Chem. Soc.* **2011**, *133*, 18003−18005. (b) Kar, C.; Adhikari, M. D.; Ramesh, A.; Das, G. NIR- and FRET-Based Sensing of Cu²⁺ and S²⁻ in Physiological Conditions and in Live Cells. *Inorg. Chem.* **2013**, *52*, 743−752.

(45) (a) Fu, Y.; Feng, Q.-C.; Jiang, X.-J.; Xu, H.; Li, M.; Zang, S.-Q. New fluorescent sensor for Cu²⁺ and S²- in 100% aqueous solution based on displacement approach. *Dalton Trans.* **2014**, *43*, 5815−5822. (b) Paul, A.; Anbu, S.; Sharma, G.; Kuznetsov, M. L.; da Silva, M. F. C. G.; Koch, B.; Pombeiro, A. J. L. Intracellular detection of Cu²⁺ and S²⁻ ions through a quinazoline functionalized benzimidazole-based new fluorogenic differential Chemosensor. *Dalton Trans.* **2015**, *44*, 16953−16964. (c) Tang, L.; Cai, M.; Huang, Z.; Zhong, K.; Hou, S.; Bian, Y.; Nandhakumar, R. Rapid and highly selective relay recognition of Cu(II) and Sulfide ions by a simple benzimidazole-based fluorescent sensor in water. *Sens. Actuators, B* **2013**, *185*, 188−194. (d) Hou, F.; Huang, L.; Xi, P.; Cheng, J.; Zhao, X.; Xie, G.; Shi, Y.; Cheng, F.; Yao, X.; Bai, D.; Zeng, Z. A Retrievable and Highly Selective Fluorescent Probe for Monitoring Sulfide and imaging in Living Cells. *Inorg. Chem.* **2012**, *51*, 2454−2460.

(46) Singh, P.; Singh, H.; Bhargava, G.; Kumar, S. Triple-Signaling mechanisms-based three-in-one multi-channel Chemosensor for discriminating Cu²⁺, acetate and ion pair mimicking AND, NOR, INH and IMP logic functions. *J. Mater. Chem. C* **2015**, *3*, 5524−5532.

(47) Wang, S.; Men, G.; Zhao, L.; Hou, Q.; Jiang, S. Binaphthyl-derived salicylidene Schiff base for dual-channel sensing of Cu, Zn, cations and integrated molecular logic gates. *Sens. Actuators, B* **2010**, *145*, 826−831.

(48) Bhardwaj, S.; Maurya, N.; Singh, A. K. Chromone based Fluorescent Organic Nanoparticles for High-Precision *in-situ* sensing of Cu²⁺, and CN⁻ ions in 100% Aqueous Solutions. *Sens. Actuators, B* **2018**, *260*, 753−762.

(49) Parua, S. P.; Sinha, D.; Rajak, K. K. A Highly Selective "On-Off-On" Optical Switch for Sequential Detection of Cu²⁺ and S²⁻⁻ Ions Based on 2, 6-Diformyl-4-methyl Phenol and Catecholase Activity by Its Copper Complex. *ChemistrySelect* **2018**, *3*, 1120−1128.

(50) Kumawat, L. K.; Kumar, M.; Bhatt, P.; Sharma, A.; Asif, M.; Gupta, V. K. An easily accessible optical chemosensor for Cu²⁺ based

on novel imidazoazine framework, its performance characteristics and potential applications. *Sens. Actuators, B* **2017**, *240*, 365−375.

(51) Zhao, Y.-C.; Chen, C.; Chen, B.; Wang, P.-Y.; Wu, Z.-B.; Li, H.; Song, B.-A.; Yang, S. Tunable fluorescent probes for selective detection of copper(II) and sulphide with completely different modes. *Sens. Actuators, B* **2017**, *241*, 168−173.

(52) Sun, M.; Yu, H.; Li, H.; Xu, H.; Huang, D.; Wang, S. Fluorescence Signaling of Hydrogen Sulfide in Broad pH Range Using a Copper Complex Based on BINOL-Benzimidazole Ligands. *Inorg. Chem.* **2015**, *54*, 3766−3772.

(53) *SAINT*, version V7.60A, Bruker, Bruker AXS Inc.: Madison, Wisconsin, USA, 2009.

(54) *SADABS*, version 2008/1, Bruker, Bruker AXS Inc.: Madison, Wisconsin, USA, 2008.

(55) Sheldrick, G. M. *Acta Crystallogr., Sect. A: Found. Adv.* **2015**, *71*, 3−8.